
Hiroshima University Institutional Repository

Molecular-level Pictures of Chemical and Structural Transformations of Mg-Al Layered Double Hydroxide Crystals (Mg/Al = 2) at Elevated Temperatures

*Kaito Matsuda [a] ‡, Ayaka Okuda [a] ‡, Mio Kawashimo [a], Ryota Fukuzaki [a], Nana Iio [a], Naoki Tarutani [a], Kiyofumi Katagiri [a], and Kei Inumaru [a] **

[a] Graduate School of Advanced Science and Engineering, Hiroshima University, 1-4-1, Kagamiyama, Higashihiroshima, Hiroshima 739-8527, Japan.

‡These authors contributed equally.

Corresponding Author

Kei Inumaru, Email: inumaru@hiroshima-u.ac.jp

KEYWORDS layered structure, CO_2 adsorbent, carbonate ions, intercalation, dehydroxylation, dehydration

ABSTRACT: Mg-Al layered double hydroxides (Mg-Al LDHs) are crystalline compounds with layered structures composed of hydroxide layers and interlayer anions such as CO_3^{2-}. The detailed understanding of the thermal decomposition behaviors is indispensable for materials design toward promising applications such as CO_2 adsorbents. Here we report that the thermal decomposition behavior of a well-crystallized Mg-Al LDH having an Mg/Al atomic ratio of 2, where all hydroxyl groups experience an identical chemical environment, provides quantitative evidence for and clear molecular-/atomic-level pictures of the multi-step transformation of the crystals at elevated temperature. Thermal decomposition is found to occur in multi-steps of 1) release the interlayer water, 2) dehydroxylation of just one-third of hydroxyl groups accompanied by formation of coordinatively unsaturated sites followed by coordination of carbonate to metals, and 3) collapse of the layered structure at higher temperature. The stepwise structural transformations are not ascribable to different coordination environments of hydroxyl groups. The reason is possibly that the structure after the partial dehydroxylation of the metal hydroxide layers is rather stable. Structural optimization by first-principles DFT calculations and its powder X-ray diffraction simulation supported the interpretations for and the molecular-level pictures of the structural transformation. These results resolve the various interpretations on the structural change of the crystals.

INTRODUCTION

Layered double hydroxides (LDHs) are layered compounds that have been known for a long time[1] but have recently been attracting much attention owing to their wide variety of advanced functions. Layered nickel hydroxides and Fe-containing LDHs are promising as electrode catalysts for water oxidation.[2,3] Solid base catalysis for organic chemical reactions,[4-6] photocatalysis for CO_2 reduction,[7,8] and ion storage materials[9] are also important research fields for green chemistry and sustainable energies. Recently developed techniques have enabled the synthesis of LDH nanomaterials such as nanocrystals[10-13] and nanosheets.[14] Composite materials containing LDH have been reported to be promising as supercapacitors[15] and high gas barrier coatings.[16]

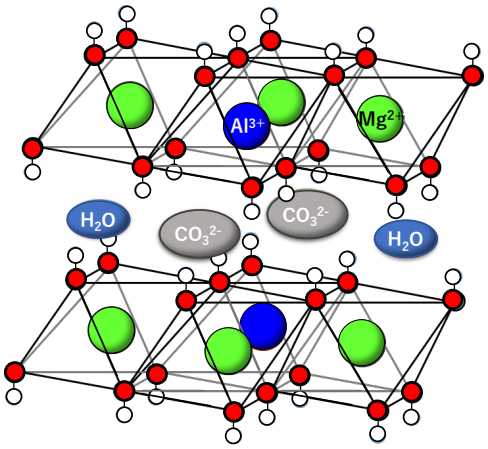

Figure 1. Illustration of Mg-Al LDH structure.

Mg-Al LDH, with the chemical formula $[Mg_{1-x}Al_x(OH)_2]^{x+}$ $[A^{n-}_{x/n}] \cdot m\ H_2O$, has also been studied for a long time from the viewpoints of both crystal chemistry and applications. The metal hydroxide layers are positively charged and the interlayer anions A^{n-} neutralize the charge.[1] Figure 1 shows a schematic illustration of Mg-Al LDH (here the anions are CO_3^{2-}). The

anions form stable hydrogen bonding networks with water molecules in the interlayer spaces.[9,17] The "memory effect" seems to be a significant reason why the crystal chemistry of LDH is attractive and mysterious: the layered crystal structure of Mg-Al LDH decomposes at above approximately 650 K, with the evolution of gaseous CO_2 and water vapor, to form a Mg-Al mixed oxide with a rock salt structure, and the oxide readily reproduces the LDH layered structure in the presence of water at ambient temperature as if it has memorized the original layered structure. The mechanism of this "memory effect" remains a controversial topic.[18] Furthermore, the details of the structural transformation of Mg-Al LDH at the lower temperature range also remain obscure. Many studies have reported the multistep structural transformation of Mg-Al LDH accompanied by the evolution of water vapor.[19-23] However, the interpretation of this transformation is ambiguous. For example, water vapor evolution at approximately 473 K (here we call this the 1st step) is sometimes ascribed to the loss of hydroxide groups associated with Al (Al-OH), and water evolution at higher temperature (the 2nd step at ca. 580 K) is assigned to the loss of Mg-OH.[21] In other studies, the 2nd step has been ascribed to that of Al-OH and the 3rd step (above 650 K) is associated with Mg-OH,[22] and *vice versa*.[23] Moreover, the interlayer distance significantly changes during these steps but its interpretation, from the crystal structural aspect, has remained unclear for a long time.[19-23] Many of these previous studies used Mg-Al LDH samples with Mg/Al atomic ratio of 3.

Here we report that by using a well-crystallized Mg-Al LDH sample having an Mg/Al atomic ratio of 2, we obtain a clear interpretation of the structural transformation steps with quantitative evidence by means of gas evolution measurements during thermal decomposition, thermogravimetric analysis (TGA), *in situ* Fourier transform infrared spectroscopy (FT-IR) and *in situ* X-ray powder diffraction (XRD) combined with first-principles calculations. The

advantage of the sample with Mg/Al atomic ratio of 2 is simplicity of the structure. Figure 2 summarizes the strategy we took in this study. As shown in Fig. 2(c), samples with Mg/Al=3 have inevitable structural complexity such as possible different metal ion arrangements in the layers and coexisting different coordination environments of hydroxide groups. On the other hand, in the structure of LDH with Mg/Al=2, each hydroxyl group coordinates to two Mg ions and one Al ion (Fig. 2(b)) (Note that Al ions do not occupy neighboring sites in the layer). That

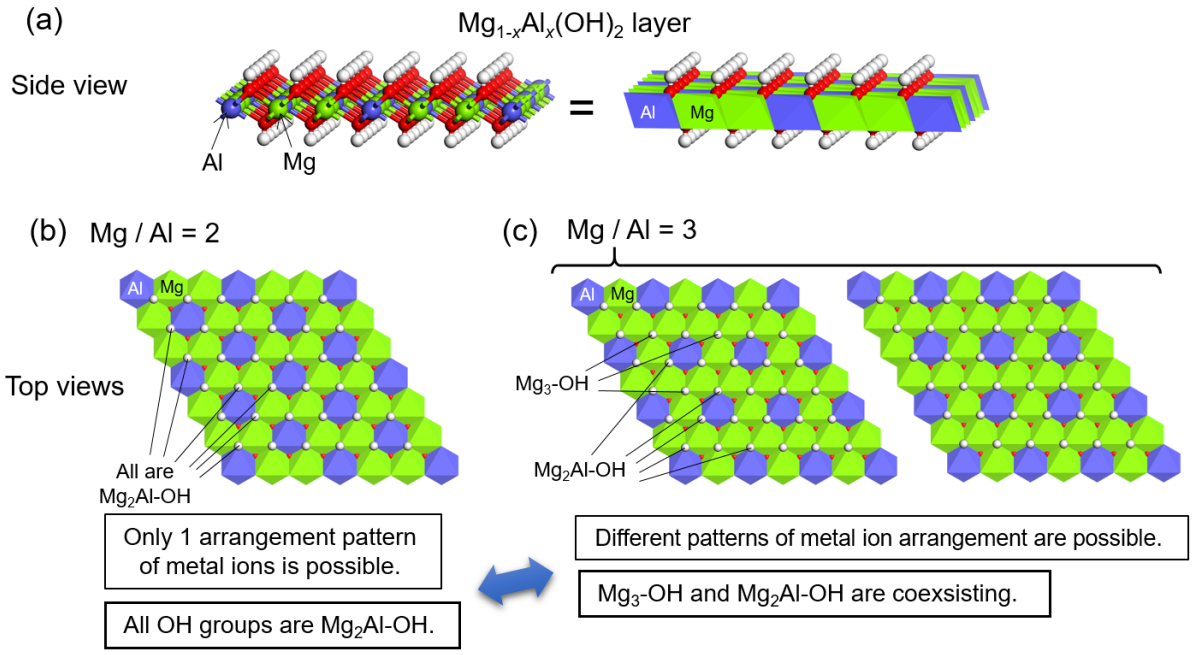

Figure 2. Structure of Mg-Al LDH with different Mg/Al atomic ratios. (a) Side view of an $Mg_{1-x}Al_x(OH)_2$ layer slab in Mg-Al LDH crystal structure. (b) Top view of an $[Mg_2Al(OH)_6]^+$ layer slab (Mg/Al = 2). (c) Top views of $[Mg_3Al(OH)_8]^+$ layer slabs (Mg/Al = 3) with different metal ion arrangements.

is, all hydroxide ions experience an identical chemical environment and the difference of Mg-OH and Al-OH is meaningless. This simplicity enables us to obtain clear molecular-/atomic-level pictures of the structural transformation based on experimental evidence and DFT calculations. These insights are useful for designing novel and promising adsorbents and catalysts based on the crystal structure and characteristic behavior of this material.

METHODS

Mg-Al LDH was synthesized by a hydrothermal method according to the report of Okamoto et al.[24] Crystallinity and purity of the sample were high judging from XRD pattern and SEM images as shown in Figures 3 and S1. The Mg/Al atomic ratio of the LDH was determined with an inductively coupled plasma (ICP) spectrometer (Thermo Fisher Scientific iCAP 6000). Evolution rates of gas molecules from the sample upon heating were measured using a gas flow system equipped with a Q-mass spectrometer. The sample (30 mg) was set in a quartz tube reactor and heated at a temperature ramp rate of 10 K min^{-1} up to 873 K under an Ar flow (100 cm^3 min^{-1}). The gas from the outlet was analyzed with the Q-mass spectrometer. The absolute value of the CO_2 evolution rate was calibrated using a standard gas, whereas that of H_2O was expressed by the Q-mass signal intensity because H_2O molecules strongly adsorbed on the inner walls of the apparatus. Separately, TGA was also used to obtain quantitative information about the desorbed gases during heating of the sample. The composition formula of the LDH sample was determined by combining the results from ICP, TPD and TG-DTA. The amount of interlayer CO_3^{2-} was assumed to be half the total of Al atoms considering the charge balance. *Ex situ* or *in situ* X-ray powder diffraction (XRD or *in situ* XRD) was performed with a D8 Advance diffractometer (Bruker), using an *in situ* sample chamber (Anton-Paar TTK-450) if necessary. Cu

Kα radiation was used for the XRD measurements. *In situ* Fourier transform infrared absorption spectroscopy (*in situ* FT-IR) was performed using an FT-IR 4200 (JASCO) spectrometer combined with a glass cell connected to a vacuum system. *In situ* XRD and *in situ* FT-IR were used to collect data at elevated temperatures in a vacuum. Structural optimization of the structural models was carried out by first-principles DFT calculations (CASTEP 2020). The shape of the unit cell of the initial model employed in the calculation is hexagonal type and contains two layers. In order to reproduce the arrangement pattern of Mg and Al ions in the layer shown in Fig. 2(b), 6 x 6 supercell in the *a* and *b* directions were constructed. Thus, the cell parameters of the initial model was a = 18.276 Å, b = 18.276 Å, c = 13.500 Å, α = 90˚, β = 90˚, and γ = 120˚. In the structural optimization, Monkhorst-Pack grid with 2×2×2 was employed and the plane wave basis set cut-off was set to 571.4 eV. No symmetry was assumed (space group: P1), and positions of all atoms (48 Mg, 24Al, 156 O, 12 C and 96 H) and all cell parameters were finally optimized. OTFG ultrasoft pseudopotentials, GGA, PBESolid fractional and TS method for DFT-D correction was used as they are implemented in CASTEP 2020. In order to simulate Infrared spectrum of a carbonate ion, linear response or density functional perturbation theory[25.26] implemented in CASTEP 2020 was applied to a CO_3^{2-} ion in the optimized structure model (Figure S4). In the calculation, Monkhorst-Pack grid with 1×1×1 was employed and the plane wave basis set cut-off was set to 900.0 eV. Norm conserving pseudopotentials were used. Simulated powder X-ray diffraction pattern was calculated using Diamond 3.2 software package for the crystal structure obtained by the DFT calculations.

RESULTS AND DISCUSSION

Figure 3 shows the XRD pattern of the Mg-Al LDH sample. The sample was prepared by a hydrothermal method.[24] Sharp diffraction peaks assigned to the basal planes (003 and 006) were clearly observed (Fig. 3(a)). Owing to the preferred orientation of the well-developed plate-like particles (see SEM images of the sample in Fig. S1 in the Supporting Information), the diffraction peaks other than those from the crystal planes parallel to the layer were rather weak. The magnified XRD pattern (Fig. 3(b)) shows that the other diffraction peaks were very sharp, which indicated the LDH sample was highly crystalline. The lattice constants were refined using the *d* spacing calculated from the peaks observed in Fig. 3 (a = 3.048(1) Å, c = 22.74(1) Å). The metal composition (Mg/Al atomic ratio) of the sample was determined to be 1.93 by ICP analysis.

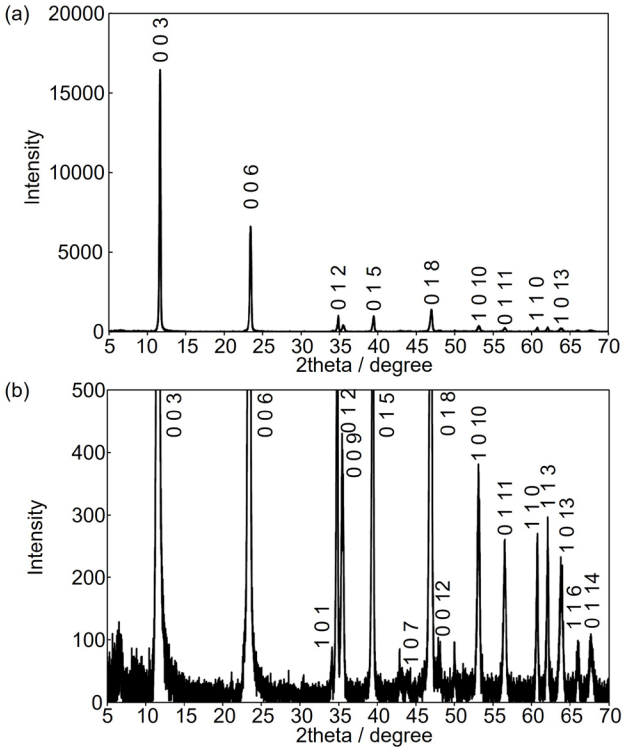

Figure 3. XRD patterns of the Mg-Al LDH sample.

(a) The whole pattern and (b) magnified pattern.

The Mg-Al LDH with a Mg/Al atomic ratio = 3 is known to readily form when the sample is prepared by the conventional co-precipitation method.[1] However, the chemical analysis in the present study gave a value of Mg/Al = 2. According to the literature,[27] the lattice constant *a* is a function of the Mg/Al ratio. That is, because the ionic radius of Mg is larger than that of Al, the lattice constant *a* increases as the Mg/Al ratio increases. The value of *a* = 3.048 Å corresponds to an Mg/Al of approximately 2 (ref. 27), which is consistent with the chemical analysis result mentioned earlier.

The profiles of the gas evolution rates during thermal decomposition experiment are shown in Figure 4(a). The gas evolution rates of H_2O and CO_2 were measured by the Q-mass spectrometer. The ordinates correspond to the gas evolution rates of H_2O and CO_2 from the sample during heating at 10 K min^{-1}. One step of CO_2 desorption at higher temperature and three steps of H_2O

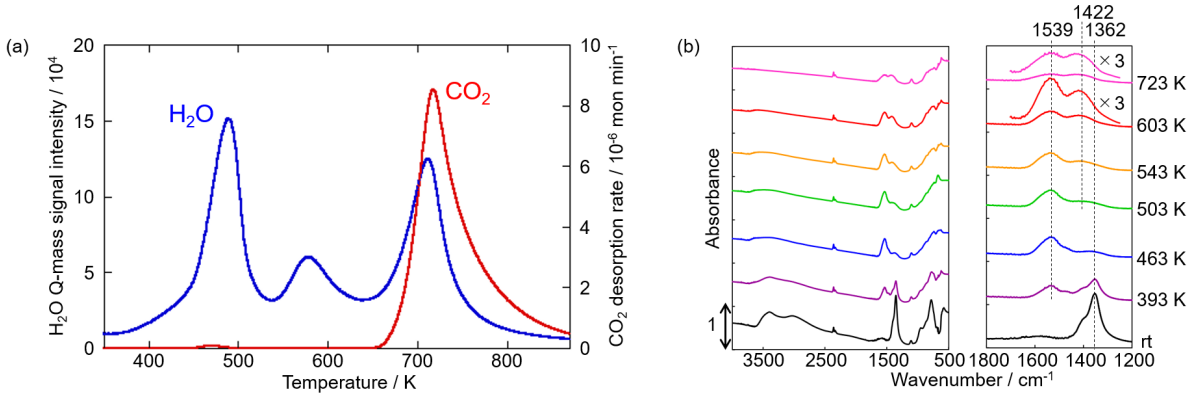

Figure 4. (a) CO_2 and H_2O gas evolution rate profiles from LDH sample as functions of sample temperature during heating at constant temperature ramp rate. (b) *In situ* FT-IR spectra of LDH in vacuum at elevated temperatures. Left and right panels show the whole and magnified ranges of wavenumbers, respectively.

desorption were observed, where the CO_2 desorption took place at the same time as the third step of H_2O desorption. This step corresponds to the collapse of the layered crystal structure.[19-21] At lower temperature, there were two steps of H_2O evolution at approximately 473 and 573 K. These steps were clearly resolved and each of them should be ascribable to different chemical transformations of the layered crystal. A trace amount of CO_2 evolution was observed at around 473 K. Its origin is unknown, and one possibility is carbonate species adsorbed on outer-surfaces of LDH crystallites.

Further investigation was carried out regarding the multi-step chemical transformation of the crystals: *in situ* FT-IR results are shown in Figure 4(b). In the FT-IR spectrum at room temperature, a strong peak with a shoulder was observed at 1362 cm^{-1}. According to the literature,[26] this peak was assigned to CO_3^{2-} anions hydrogen bonded to interlayer water molecules. At 463 K, the peak at 1362 cm^{-1} disappeared and a new peak emerged at 1539 cm^{-1}. The peak shift to a higher wavenumber was interpreted as a result of a loss of the hydrogen

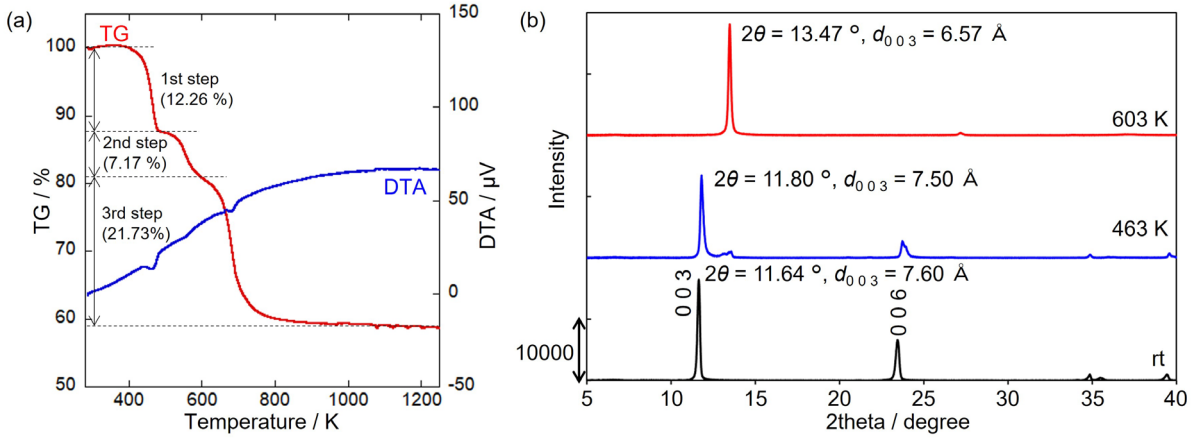

Figure 5. (a) TG analysis of the Mg-Al LDH samples. The temperature ramp rates are 3 K min^{-1}. DTA data showed that all weight-loss steps were endothermic processes. (b) *In situ* XRD patterns of Mg-Al LDH.

bonds. The single peak at 1539 cm^{-1} indicated that the carbonate ions were in a highly symmetrical chemical environment: almost all hydrogen bonds to interlayer water were broken at 463 K. At 603 K, the spectrum exhibited two separate peaks at 1539 and 1422 cm^{-1}. The split peaks indicated a lower symmetrical chemical environment, such as carbonates coordinating to metal ion(s). The peak split is known to significantly depend on the coordination structure of the carbonate species:[28,29] in the case of monodentate carbonate species, the split between the two peaks is less than 300 cm^{-1} and bidentate species give a split of more than 300 cm^{-1}. The experimental value of the split was 117 cm^{-1} in the spectrum at 603 K (Fig. 3(b)), which indicated the carbonate species was monodentate above 603 K, i.e., after the 2nd step of H_2O desorption, being consistent with an earlier theoretical calculation.[30]

These results led to the straightforward insights that the 1st step corresponds to desorption of interlayer water molecules and the 2nd step is ascribed to partial dehydroxylation of the metal hydroxide layers to form coordinatively unsaturated sites followed by coordination of the carbonate species to them.

TGA gives quantitative data of the chemical transformation of the crystals. Especially, the chemical environment of hydroxyl groups was uniform in the present sample, as mentioned above, so the information is expected to be powerful for a clear insight into the chemical reactions. Three steps of weight loss were clearly observed in the TGA results shown in Figure 5(a) and Figure S2. The 1st, 2nd and 3rd steps corresponded to 12.3, 7.2 and 21.7% of the initial weight, respectively (Fig. 5(a)). Expecting that the stepwise transformations are well resolved, we used TGA data with a slow temperature ramp rate of 3 K min^{-1}. Actually it was confirmed that these values were not sensitive to the different temperature ramp rates (3 and 10 K min^{-1}), as shown in Fig. S2. Here, it should be noted that, according to Fig. 4(a), the 1st and 2nd steps of

the weight loss were purely ascribed to H_2O desorption, while the 3rd step included CO_2 desorption as well as that of H_2O. It should be noted that the sample consists of well-developed crystallites and BET surface area of this sample is as small as 5.8 $m^2\ g^{-1}$. From this value and molecular cross-sectional area of H_2O (0.125 nm^2) the monolayer adsorption amount of water V_m is calculated to be 7.7 x 10^{-5} mol g^{-1}. In prior to the measurements of the gas evolution (Fig. 4(a)) and the TGAs (Fig. 5(a) etc), the sample was exposed to a dry gas flow (Ar or N_2) in the apparatus at room temperature for enough time (ca. 1 h) to minimize physisorbed water. That is, it is not likely that the surfaces of the sample are covered by thick physisorbed water multilayers in these conditions. Here, the monolayer adsorption amount V_m is as small as 1.1% of the H_2O observed in the 1st step. Thus, the TG results are assigned to the amount of interlayer water at the 1st step (Table 1) and the amount of partial dehydroxylation at the 2nd step. The interlayer water amount (1.61) was close to the value calculated from the occupation of interlayer spaces (1.5)(ref. 31). The change of the chemical formula (composition) for each step is shown in Scheme 1.

Table 1. Properties of the LDH sample

Mg / Al	1.93
Chemical formula	$Mg_{1.98}Al_{1.02}(OH)_6 \cdot 0.51\ CO_3 \cdot 1.61\ H_2O$
Lattice constant a	3.048 (1) Å
Lattice constant *c*	22.74 (1) Å
Interlayer distance	7.58 Å

Scheme 1. Change of composition of the LDH sample in each step

$Mg_{1.98}Al_{1.02}(OH)_6 \cdot 0.51\ CO_3 \cdot 1.61\ H_2O$

↓ $- H_2O$ (1st step, up to 503 K)

$Mg_{1.98}Al_{1.02}(OH)_6 \cdot 0.51\ CO_3$

↓ $- H_2O$ (2nd step, up to 603 K)

$Mg_{1.98}Al_{1.02}(OH)_{4.11}O_{0.95} \cdot 0.51\ CO_3$

↓ $- H_2O, - CO_2$ (3rd step, above 643 K)

$Mg_{1.98}Al_{1.02}O_{3.51}$

Here it should be noted that the amount of dehydroxylation at the 2nd step was very close to one third of the hydroxyl groups: if all metal ions changed from octahedral to square pyramidal (that is, the coordination number changes from 6 to 5), just one third of the hydroxyl groups

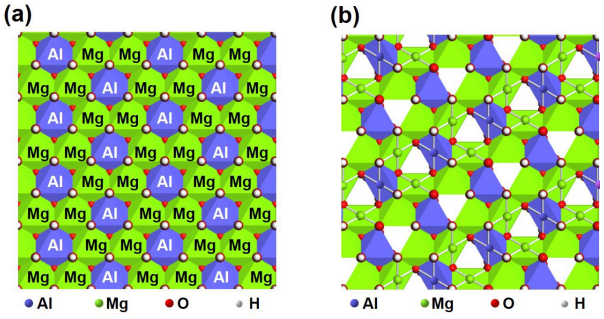

Figure 6. Top views of $[Mg_2Al(OH)_6]^+$ layer slab (Mg/Al = 2) (a) and idealized partially dehydroxylated layer $[Mg_2Al(OH)_4O]^+$ (b).

should be lost. One of the ideal structures of the hydroxide layer is shown in of Figure 6(b). Two Mg ions and one Al ion form one coordinatively unsaturated site, and the number of coordinatively unsaturated sites is twice that of carbonate ions (i.e. Mg_2Al / CO_3^{2-} ~2). Thus each carbonate ion can form a monodentate species by coordinating to two Mg and one Al ions using one unsaturated site.

To obtain information about the crystal structure during heating, *in situ* XRD measurements were carried out at elevated temperatures in a vacuum. The results are shown in Figure 5(b). At room temperature, sharp peaks, indexed as 003 and 006, were clearly observed (bottom black line in Fig. 5(b)). The interlayer distance was 7.60 Å. Then the sample was heated to 463 K with the expectation to observe the structural change induced by the 1st step of H_2O desorption at approximately 473 K, as shown in Fig. 4 (Note that the sample temperature was constant for each measurements in Figs. 4(b) and 5(b), whereas temperature was continuously elevated in Figs. 4(a) and 5(a)). As shown by the blue line in the middle of Fig. 5(b), the interlayer distance decreased only slightly by 0.1 Å. Another observation is that the 006 peak was significantly weakened compared with the pattern obtained at room temperature. Next, the sample was heated to 603 K. This temperature corresponded to that slightly higher than the 2nd H_2O evolution step at approximately 573 K. The XRD pattern (top red line in Fig. 5(b)) showed that the peak from the basal plane (003) remained strong, and the interlayer distance drastically decreased by 0.93 Å to 6.57 Å. The intensity of the 006 diffraction peak decreased further.

The *in situ* XRD experiments demonstrated two important things: (1) after the 2nd step, the layered structure of the crystals is maintained, and (2) the interlayer distance drastically decreases before and after the 2nd step (i.e. partial dehydroxylation of the layers). The *in situ* FT-IR revealed that, after the 2nd step, the carbonate ions formed monodentate species. On the basis

of all the information combined, a structural model was constructed and all atomic positions and cell parameters were optimized by first-principles DFT calculations. Vibrational spectra were also calculated and compared with the *in situ* FT-IR results.

The structurally optimized model after the partial dehydroxylation (i.e., after the 2nd step) is shown in Figures 7 and S3. All carbonate species formed monodentate species by coordinating to two Mg and one Al ions using half of the coordinatively unsaturated sites generated by the dehydroxylation of the layers. Calculation of the vibrational spectrum was also performed using a model in Figure S4, and the result is shown in Figure S5. The carbonate species gave two split peaks at 1537 and 1373 cm^{-1} in the calculated spectrum. Note that the split width of these two values was in the range of the monodentate species (<300 cm^{-1}).[29] These peak positions calculated from the model were close to those in the experimental spectrum (1539 and 1422 cm^{-1}). Furthermore, the interlayer distance optimized in the first-principles calculation (6.39 Å) was similar to the experimental value (6.57 Å in Fig. 5(b)). The evidence obtained in the present study demonstrated that the stepwise dehydroxylation (i.e. the 2nd and 3rd steps) are not ascribable to different coordination environments of hydroxyl groups in the initial structure. The reason is possibly that the structure after the 2nd step (Fig. 7 and Fig. S3) is rather stable.

Finally, we simulated the powder X-ray diffraction pattern based on the crystal structure in Fig. 7, and compared the result to the experimental diffraction pattern. Figure 8 compares the simulated and experimentally obtained diffraction patterns. The experimental pattern in Fig. 8 (bottom panel) is identical with *in situ* data at 603 K in Fig. 5(b). Because of the strong preferred orientation of the sample, the diffraction peaks other than those from the crystal planes parallel to the layer are rather weak in the experimental data (the bottom panel in Fig. 8). As mentioned above (Fig. 5(b)), significant decrease of 006 diffraction intensity was observed when the sample

was heated at 603 K (see the very weak diffraction peak at 2θ=27.2˚ in Fig. 5(b) and the bottom panel in Fig. 8), while the sample before heating (i.e. room temperature) gave a strong 006

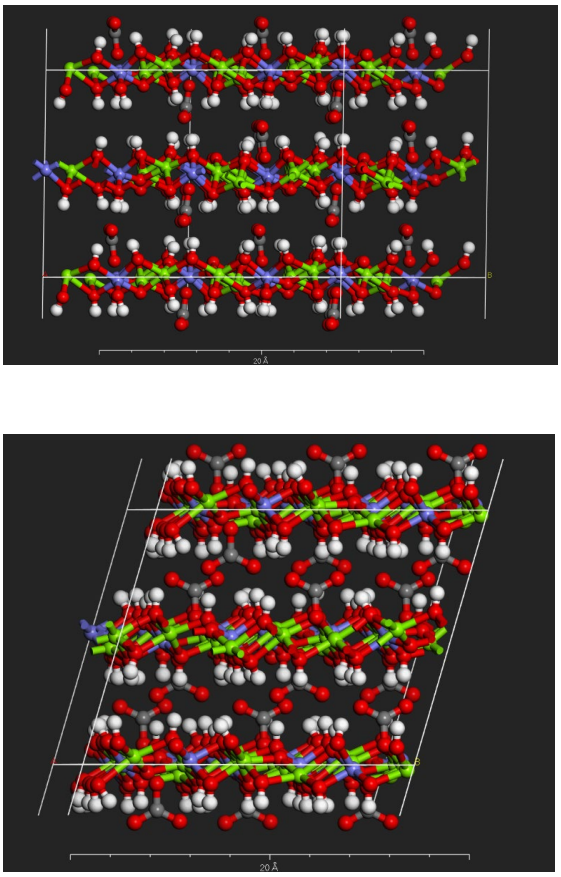

Figure 7. Structurally optimized crystal model of partially dehydroxylated LDH $Mg_2Al(OH)_4O \cdot 0.5\ CO_3$. This structure corresponds to the crystal after the partial dehydroxylation of the layers (after the "2nd step" of water vapor evolution).

Al: blue, Mg: green, O: red, C: grey, H: white.

diffraction peak at around 2θ=23.4˚ (the bottom black pattern in Fig. 5(b)). Here the crystal structure shown in Fig. 7 was used to simulate the powder X-ray diffraction. The simulation successfully reproduced the significant decrease of the 006 peak observed in the experiments: the intensity ratio I_{006} / I_{003} in the experimental data decreased to as low as 0.02 upon heating at 603 K (Fig. 5(b) and the bottom panel of Fig. 8), and the simulation gave the corresponding intensity ratio I_{004} / I_{002} to be 0.03 accordingly. Here, note that the interlayer distance corresponds to 003 diffraction in the experimental data (bottom panel in Fig. 8), whereas that corresponds to 002 in the simulated data (top panel in Fig. 8). The difference is due to the different sizes of unitcells assumed. The good agreements of the model in Fig. 7 obtained by purely first-principles

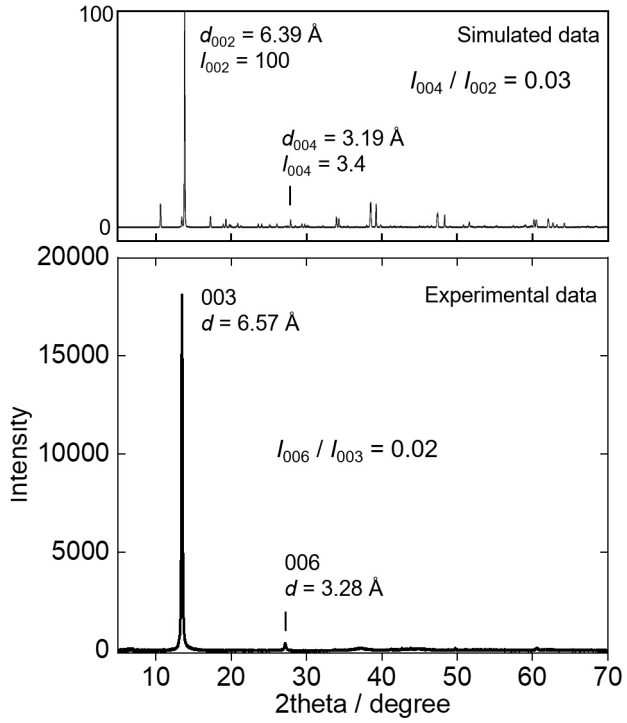

Figure 8. Comparison of powder X-ray diffraction patterns based on simulation using the crystal structure obtained by the first-principles DFT calculations (top panel) and experimental *in situ* measurement at 603 K (bottom panel).

calculation with experimental data (*d* spacing and change in the X-ray diffraction intensity) strongly support the present interpretations for and the molecular-level pictures of the structural transformation of LDHs.

Furthermore, the simulation result of powder X-ray diffraction supports the following interpretation regarding the change of the diffraction intensity ratio I_{006} / I_{003} in Fig. 5(b): The LDH sample in the ambient temperature contains a large amount of water molecules and carbonate ions in the interlayer spaces. These molecules and ions bring about a large electron density at the center of the interlayer spaces. Since X-ray diffraction pattern is a kind of Fourier transform of electron density in the real space, the high electron density at the center of interlayer spaces result in a strong diffraction intensity corresponding to the periodicity of half interlayer distance. On the other hand, in the structure shown in Fig. 7 after the 2nd step of the structural transformation, interplanar water molecules are removed and the carbonate ions move to deviate their positions from the center of interlayer spaces. Thus, the electron density at the center of the interlayer spaces decreases and this change in electron density brings about the decrease of 006 diffraction intensity whereas the layered structure is remained as is demonstrated by the strong 003 diffraction.

CONCLUSIONS

In conclusion, quantitative investigation of a well-crystallized Mg-Al LDH sample having an Mg/Al atomic ratio of 2, molecular-/atomic-level pictures of the structural transformation at elevated temperature were successfully obtained: chemical transformations such as dehydration, dehydroxylation, formation of coordinatively unsaturated sites, and coordination of carbonate to metals interplay in the crystal. The stepwise structural transformation are not ascribable to

different coordination environments of hydroxyl groups in the initial structure. The reason is possibly that the structure after the partial dehydroxylation of the metal hydroxide layers is rather stable. These interpretations were supported by structural full optimization of the partially dehydroxylated layered structural model by the first-principles DFT calculations as well as a simulation of powder X-ray diffraction based on the structural model. These results provide important information on crystal chemistry of LDH, as well as useful insights for designing novel and promising adsorbents and/or catalysts on the basis of the crystal structure and characteristic behavior of this material. We expect that this work stimulate further studies on the materials from both sides of experiments and theoretical calculations.

ASSOCIATED CONTENT

Supporting Information

The Supporting Information is available free of charge at .....

SEM images, TG-DTA data, structural optimization results of the material by first-principle DFT calculation, structural model for IR spectrum simulation, and IR spectrum simulation result.

AUTHOR INFORMATION

Corresponding Author

Kei Inumaru – Graduate School of Advanced Science and Engineering, Hiroshima University, 1-4-1, Kagamiyama, Higashihiroshima, Hiroshima 739-8527, Japan; orcid.org/0000-0001-6876-3854; Email: inumaru@hiroshima-u.ac.jp

Authors

Kaito Matsuda[‡] – Graduate School of Advanced Science and Engineering, Hiroshima University, 1-4-1, Kagamiyama, Higashihiroshima, Hiroshima 739-8527, Japan.

Ayaka Okuda[‡] – Graduate School of Advanced Science and Engineering, Hiroshima University, 1-4-1, Kagamiyama, Higashihiroshima, Hiroshima 739-8527, Japan.

Mio Kawashimo – Graduate School of Advanced Science and Engineering, Hiroshima University, 1-4-1, Kagamiyama, Higashihiroshima, Hiroshima 739-8527, Japan.

Ryota Fukuzaki – Graduate School of Advanced Science and Engineering, Hiroshima University, 1-4-1, Kagamiyama, Higashihiroshima, Hiroshima 739-8527, Japan.

Nana Iio – Graduate School of Advanced Science and Engineering, Hiroshima University, 1-4-1, Kagamiyama, Higashihiroshima, Hiroshima 739-8527, Japan.

Naoki Tarutani – Graduate School of Advanced Science and Engineering, Hiroshima University, 1-4-1, Kagamiyama, Higashihiroshima, Hiroshima 739-8527, Japan; orcid.org/0000-0003-0696-8082

Kiyofumi Katagiri – Graduate School of Advanced Science and Engineering, Hiroshima University, 1-4-1, Kagamiyama, Higashihiroshima, Hiroshima 739-8527, Japan; orcid.org/0000-0002-9548-9835

Author Contributions

‡These authors contributed equally.

Notes

The authors declare no competing financial interests.

ACKNOWLEDGMENT

This work was partly supported by JSPS KAKENHI Grand Number JP18H01709,JP23H00236, JP23KJ1624, JST ACT–C Grant Number JPMJCR12Y2, and JST-Mirai Program Grant Number JPMJMI22E3.

REFERENCES

(1) *Layered Double Hydroxides (Structure and Bonding, 119);* Duan, X., Evans, D. G., Eds.; Springer: Berlin, 2006.

(2) Burke, M. S.; Kast, M. G.; Trotochaud, L.; Smith, A. M.; Boettcher, S. W. Cobalt-Iron (Oxy)Hydroxide Oxygen Evolution Electrocatalysts: The Role of Structure and Composition on Activity, Stability, and Mechanism. *J. Am. Chem. Soc.*, **2015**, *137*, 3638–3648.

(3) Louie, M. W.; Bell, A. T. J. An Investigation of Thin-film Ni-Fe Oxide Catalysts for the Electrochemical Evolution of Oxygen. *Am. Chem. Soc.*, **2013**, *135*, 12329–12337.

(4) Ebitani, K.; Motokura, K.; Mori, K.; Mizugaki, T.; Kaneda, K. Reconstructed Hydrotalcite as a Highly Active Heterogeneous Base Catalyst for Carbon-Carbon Bond Formations in the Presence of Water. *J. Org. Chem.*, **2006**, *71*, 5440–5447.

(5) Cantrell, D. G.; Gillie, L. J.; Lee, F. ; Wilson, K. Structure-Reactivity Correlations in MgAl Hydrotalcite Catalysts for Biodiesel Synthesis. *Appl. Catal. A:General*, **2005**, *287*, 183–190.

(6) Nishimura, S.; Takagaki, A.; Ebitani, K. *Green Chem.*, Characterization, Synthesis and Catalysis of Hydrotalcite-Related Materials for Highly Efficient Materials Transformations. **2013**, *15*, 2026–2042.

(7) Teramura, K.; Iguchi, S.; Mizuno, Y.; Shishido, T.; Tanaka, T. Photocatalytic Conversion of CO_2 in Water over Layered Double Hydroxides. *Angew. Chem. Int. Ed.*, **2012**, *51*, 8008–8011.

(8) Iguchi, S.; Teramura, K.; Hosokawa, S.; Tanaka, T. Photocatalytic Conversion of CO_2 in an Aqueous Solution using Various Kinds of Layered Double Hydroxides. *Catal. Today*, **2015**, *251*, 140–144.

(9) Sudare, T.; Yamaguchi, T.; Ueda, M.; Shiiba, H.; Tanaka, H.; Tipplook, M.; Hayashi, F.; Teshima, K. Critical Role of Water Structure around Interlayer Ions for Ion Storage in Layered Double Hydroxides. *Nat. Commun.*, **2022**, *13*, Art. No. 6448.

(10) Tokudome, Y.; Morimoto, T.; Tarutani, N.; Vaz, P. D.; Nunes, C. D.; Prevot, V.; Stenning, G. B. G.; Takahashi, M. Layered Double Hydroxide Nanoclusters: Aqueous, Concentrated, Stable, and Catalytically Active Colloids toward Green Chemistry, *ACS Nano*, **2016**, *10*, 5550–5559.

(11) Tarutani, N.; Kimura, S.; Sakata, T.; Suzuki, K.; Kagagiri, K.; Inumaru, K. Metal Hydroxide Salt Monolayer Nanoparticles: Synthesis, Redox Characterization, and Electrochemical Catalytic Performance. *ACS Materials Lett.* **2022**, *4*, 1430–1435.

(12) Kuroda, Y.; Miyamoto, Y.; Hibino, M.; Yamaguchi, K; Mizuno, N. Tripodal Ligand-Stabilized Layered Double Hydroxide Nanoparticles with Highly Exchangeable CO_3^{2-}, *Chem. Mater.*, **2013**, *25*, 2291–2296.

(13) Muramatsu, K.; Hayashi, S.; Kuroda, Y.; Oka, Y.; Wada, H.; Shimojima, A.; Kuroda, K. Selective Covalent Modification of Layered Double Hydroxide Nanoparticles with Tripodal Ligands on Outer and Interlayer Surfaces. *Inorg. Chem.* **2020**, *59*, 6110–6119.

(14) Wang, Q.; O'Hare, D. *Chem. Rev.*, Recent Advances in the Synthesis and Application of Layered Double Hydroxide (LDH) Nanosheets. **2012**, *112*, 4124–4155.

(15) Ma, H.-N.; He, J.; Xiong, D.-B.; Wu, J.-S.; Li, Q.-Q.; Dravid, V.; Zhao, Y.-F. Nickel Cobalt Hydroxide @Reduced Graphene Oxide Hybrid Nanolayers for High Performance Asymmetric Supercapacitors with Remarkable Cycling Stability. *ACS Appl. Mater. Interfaces*, **2016**, *8*, 1992–2000.

(16) Yu, J.; Ruengkajorn, K.; Crivoi, D.-G.; Chen, C.; Buffet, J.-C.; O'Hare, D. High Gas Barrier Coating using Non-Toxic Nanosheet Dispersions for Flexible Food Packaging Film. *Nat. Commun.*, **2019**, *10*, 2398.

(17) Sasai, R.; Sato, H.; Sugata, M.; Fujimura, T.; Ishihara, S.; Deguchi, K.; Ohki, S.; Tansho, M.; Shimizu, T.; Oita, N. et al. Why Do Carbonate Anions Have Extremely High Stability in the Interlayer Space of Layered Double Hydroxides? Case Study of Layered Double Hydroxide Consisting of Mg and Al (Mg/Al = 2). *Inorg. Chem.* **2019**, *58*, 10928–10935.

(18) Mascolo, G.; Mascolo, M. C. On the Synthesis of Layered Double Hydroxides (LDHs) by Reconstruction Method Based on the "Memory Effect" *Micropor. Mesopor. Mater.*, **2015**, *214*, 246–248.

(19) Bellotto, M.; Rebours, B.; Clause, O.; Lynch, J.; Bazin, D.; Elkaïm, E. A Reexamination of Hydrotalcite Crystal Chemistry. *J. Phys. Chem.*, **1996**, *100*, 8527–8534.

(20) Bellotto, M.; Rebours, B.; Clause, O.; Lynch, J.; Bazin, D.; Elkaïm, E. Hydrotalcite Decomposition Mechanism: A Clue to the Structure and Reactivity of Spinel-Like Mixed Oxides. *J. Phys. Chem.*, **1996**, *100*, 8535–8542.

(21) León, M.; Díaz, E.; Bennici, S.; Vega, A.; Ordóñez, S.; Auroux, A. Adsorption of CO_2 on Hydrotalcite-Derived Mixed Oxides: Sorption Mechanisms and Consequences for Adsorption Irreversibility. *Ind. Eng. Chem. Res.*, **2010**, *49*, 3663–3671.

(22) Yang, W.; Kim, Y.; Liu, P. K. T.; Sahimi, M.; Tsotsis, T. T. A Study by In Situ Techniques of the Thermal Evolution of the Structure of a Mg-Al-CO_3 Layered Double Hydroxide. *Chem. Eng. Sci.*, **2002**, *57*, 2945–2953.

(23) Zhang, J.; Xu, Y. F.; Qian, G.; Xu, Z. P.; Chen, C.; Liu, Q. Reinvestigation of Dehydration and Dehydroxylation of Hydrotalcite-Like Compounds through Combined TG-DTA-MS Analyses. *J. Phys. Chem. C*, **2010**, *114*, 10768–10774.

(24) Okamoto, K.; Iyi, N.; Sasaki, T. Factors affecting the crystal size of the MgAl-LDH (Layered Double Hydroxide) Prepared by using Ammonia-Releasing Reagents. *Appl. Clay Sci.*, **2007**, *37*, 23–31.

(25) Baroni, S.; de Gironcoli, S.; dal Corso, A.; Giannozzi, P. Phonons and related crystal properties from density-functional perturbation theory, *Rev. Mod. Phys.,* **2001**, *73*, 515-562.

(26) Gonze, X. First-principles responses of solids to atomic displacements and homogeneous electric fields: Implementation of a conjugate-gradient algorithm, *Phys. Rev. B*, **1997**, *55*, 10337-10354.

(27) Sjåstad, A. O.; Andersen, N. H.; Vajeeston, P.; Karthikeyan, J.; Arstad, B.; Karlsson, A.; Fjellvåg, H. On the Thermal Stability and Structures of Layered Double Hydroxides $Mg_{1-x}Al_x(OH)_2(NO_3)_x \cdot mH_2O$ (0.18 <= x <= 0.38). *Eur. J. Inorg. Chem.*, **2015**, 1775–1788.

(28) Di Bitetto, A.; Kervern, G.; André, E.; Durand, P.; Carteret, C. Carbonate-Hydrogenocarbonate Coexistence and Dynamics in Layered Double Hydroxides. *J. Phys. Chem. C*, **2017**, *121*, 6104–6112.

(29) Nakamoto, K. *Infrared and Raman Spectra of Inorganic and Coordination Compounds;* John Wiley & Sons: Hoboken, 1997.

(30) Costa, D. G.; Rocha, A. B.; Souza, W. F.; Chiaro, S. S. X.; Leitão, A. A. Ab Initio Study of Reaction Pathways Related to Initial Steps of Thermal Decomposition of the Layered Double Hydroxide Compounds. *J. Phys. Chem. C*, **2012**, *116*, 13679–13687.

(31) Taylor, H. F. W. Crystal-Structures of Some Double Hydroxide Minerals. *Miner. Mag.*, **1973**, *39*, 377–389.

TOC GRAPHICS